Electron delocalization in cyanide-bridged coordination polymer electrodes for Li-ion batteries studied by soft x-ray absorption spectroscopy

Daisuke Asakura, Masashi Okubo, Yoshifumi Mizuno, Tetsuichi Kudo, Haoshen Zhou, Kenta Amemiya, Frank M. F. de Groot, Jeng-Lung Chen, Wei-Cheng Wang, Per-Anders Glans, Chinglin Chang, Jinghua Guo, and Itaru Honma

Phys. Rev. B **84**, 045117 — Published 14 July 2011

DOI: 10.1103/PhysRevB.84.045117

Electron delocalization in cyanide-bridged coordination polymer electrode for Li-ion batteries studied by soft x-ray absorption spectroscopy

Daisuke Asakura[1], Masashi Okubo[1]*, Yoshifumi Mizuno[1], Tetsuichi Kudo[1], Haoshen Zhou[1], Kenta Amemiya[2], Frank M. F. de Groot[3], Jeng-Lung Chen[4,5], Wei-Cheng Wang[4,5], Per-Anders Glans[4], Chinglin Chang[5], Jinghua Guo[4], and Itaru Honma[6]

[1] *Energy Technology Research Institute, National Institute of Advanced Industrial Science and Technology, Tsukuba, Ibaraki 305-8568, Japan*

[2] *Photon Factory, IMSS, High Energy Accelerator Research Organization, Tsukuba, Ibaraki 305-0801, Japan*

[3] *Department of Inorganic Chemistry and Catalysis, Utrecht University, Sorbonnelaan 16, 3584 Utrecht, The Netherlands*

[4] *Advanced Light Source, Lawrence Berkeley National Laboratory, Berkeley, California 94720, USA*

[5] *Department of Physics, Tamkang University, Tamsui, Taiwan 250, R. O. C.*

[6] *Institute of Multidisciplinary Research for Advanced Materials, Tohoku University, Sendai, Miyagi 980-8577, Japan*

(Dated: May 24, 2011)

The electronic structure change during the reversible Li-ion storage reaction in a bimetallic MnFe-Prussian blue analogue ($Li_xK_{0.14}Mn_{1.43}[Fe(CN)_6]\cdot 6H_2O$) was investigated by soft x-ray absorption spectroscopy. The Mn $L_{2,3}$-edge spectra revealed the unchanged Mn^{2+} high-spin state regardless of Li-ion concentration (x). On the other hand, the Fe $L_{2,3}$-edge spectra clearly revealed a reversible redox behavior as $Fe^{3+} \leftrightarrow Fe^{2+}$ states with Li-ion insertion/extraction. Experimental findings suggested strong metal-to-ligand charge transfer in accompany with ligand-to-metal one. The resulting charge delocalization between the Fe and CN is considered to contribute to the high reversibility of the Li-ion storage process.

PACS numbers: 82.47.Aa, 78.70.Dm, 71.20.Rv, 82.40.Qt

I. INTRODUCTION

Electronic properties of coordination polymers have attracted considerable attention since they have the unique potential of wide applications for spintronics, guest separation, and ion storage[1–3]. In particular, coordination polymer electrodes for Li-ion batteries exhibit the solid-state redox of the host framework during charge/discharge process[4–6] as their drastic changes in orbital occupation and energy levels of transition metals (TMs) and bridging ligands.

Recently, we demonstrated that the cyanide-bridged coordination polymer, Prussian blue analogue (PBA), undergoes electrochemical Li-ion insertion/extraction (discharge/charge) reactions with high reversibility[7]. PBAs generally have a perovskite structure bridged by cyanide groups: $A^+_y M^{2+}_{\alpha}{}_z[M^{3+}_{\beta}(CN)_6]\cdot nH_2O$ (A: alkali metal, M_α and M_β: TMs) (Fig. 1(a)). As indicated in the formula, there are Schottky defects at A and $[M_\beta(CN)_6]$ sites because alkali-metal ions with small ionic radii such as K-ion cannot stably occupy the large pore in PBAs. Thus, in contrast to M_β ions in the $M_\beta(CN)_6$ coordination environment, M_α ions form an $M_\alpha(NC)_{6-\delta}(OH_2)_\delta$ octahedron ($0 < \delta < 2$) that has a weak and slightly distorted ligand field in contrary to a perfect $M_\alpha(NC)_6$ octahedron. By using this host framework, the following electrochemical reaction can be achieved; $x\mathrm{Li}^+ + xe^- + (\mathrm{PBA})^0 \leftrightarrow \mathrm{Li}^+_x(\mathrm{PBA})^{x-}$.

Figure 1(a) shows schematic electrochemical reaction and crystal structure of $Li_xK_{0.14}Mn_{1.43}[Fe(CN)_6]\cdot 6H_2O$ (Li_xMnFe-PBA) which exhibits high reversibility over 100 charge/discharge cycles[7]. During the reaction completely via solid solution state, the Li concentration x continuoursly changes within each particle, and electrons are simultaneously supplied/removed by an electric current (Fig. 1(a)), resulting in charge/discharge process at a specific redox voltage (Fig. 1(b)).

According to the previous reports, Fe-CN-Mn PBA framework (e.g. Rb salt: $Rb_yMn_z[Fe(CN)_6\cdot nH_2O)$ exhibits rich physical properties such as inter-metallic charge transfer transition due to the strong interaction among the Mn t_{2g}, Fe t_{2g}, and CN π^* orbitals[8–10]. This suggested that MnFe-PBA could have the class II mixed valence state with electron delocalization over the entire framework, therefore the investigation of the electronic structure of MnFe-PBA during Li-ion insertion/extraction is highly intriguing. Furthermore, understanding the corresponding electronic-structure change during the redox reaction would shed light on material designs to improve the performance of the coordination polymer electrodes. Consequently, it is crucial for the research field of not only basic science but also technological applications to perform element-selective investigations of the electronic structures of PBAs.

For an element-selective observation of $3d$ electronic structures of TMs, soft x-ray absorption spectroscopy (XAS) is a powerful technique. Concerning hexacyanometalates, Cartier dit Moulin *et al.*[12] and Hocking *et al.*[13] showed that Fe $L_{2,3}$-edge ($2p_{1/2,3/2} \rightarrow 3d$ absorption) XAS for $K_3[Fe^{III}(CN)_6]$ and $K_4[Fe^{II}(CN)_6]$ in combination with the charge transfer multiplet (CTM) calculations could clarify not only the Fe oxidation state but

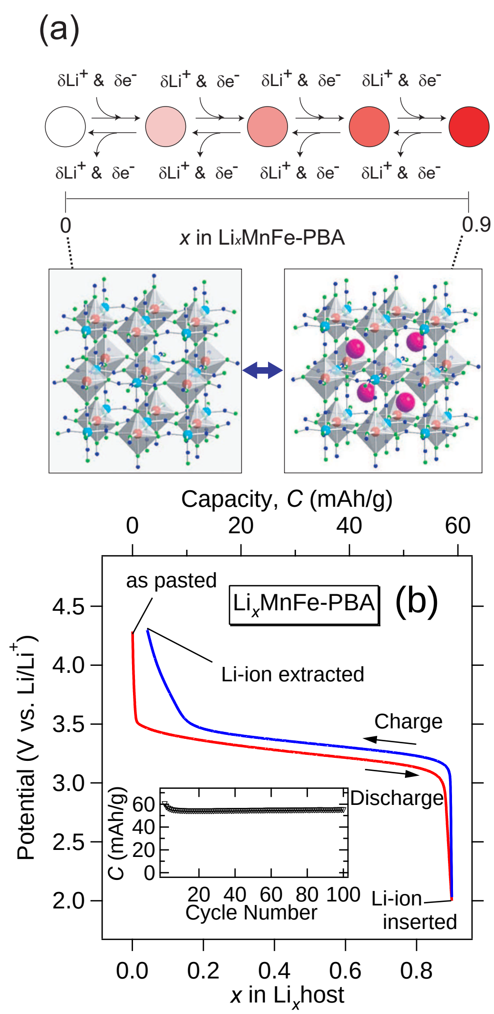

FIG. 1: (Color online) (a) Schematic electrochemical reaction and corresponding crystal structure of Li_xMnFe-PBA. The color change shows Li-ion concentration within a MnFe-PBA particle. (b) Discharge (Li-ion insertion)/charge (Li-ion extraction) curves. Li-ion concentration, x, was calculated from the integrated electric current through the electrochemical cell. The inset in (b) indicates cyclability of the discharge capacity during 100 cycles[7].

also the degrees of donation and back-donation between the Fe and cyanide ligand. Thus, XAS is an appropriate method to investigate the electronic-structure change of PBAs during the charge/discharge process. Here, we report XAS investigations of the electrochemical reversible Li-ion storage reaction in MnFe-PBA.

II. EXPERIMENT

We synthesized MnFe-PBA using the precipitation method and performed elemental analyses as previously reported[7]. X-ray diffraction measurements confirmed that the compound had a conventional cubic PBA structure without any impurity phases. For electrochemical experiments, MnFe-PBA (75 wt%), acetylene black (20 wt%), and polytetrafluoroethylene (5 wt%) were ground into a paste. The electrochemical Li-ion insertion/extraction has been performed according to Ref.[7]. As Figure 1(b) displays, MnFe-PBA can store Li ions up to $x = 0.9$, so that we prepared samples of as-pasted (MnFe-PBA, before Li-ion insertion), fully Li-ion inserted ($Li_{0.9}$MnFe-PBA), and fully Li-ion extracted (Li_0MnFe-PBA) states.

XAS measurements were performed at BL-7A of the Photon Factory (PF). The total electron-yield (TEY) mode was employed. The resolution was $E/\Delta E \sim 1500$. The pressure was maintained at the order of 10^{-8} Torr. All the XAS measurements were performed at room temperature. In advance of the XAS measurements at PF, we had done preliminary XAS measurements at BL7.0.1 of the Advanced Light Source.

III. RESULTS AND DISCUSSION

Figure 2 shows photon flux-normalized XAS spectra of Li_xMnFe-PBA at the Mn $L_{2,3}$ edges. The Mn $L_{2,3}$-edge XAS spectra of all the samples were nearly the same, which suggested that the electronic structure of Mn remains unchanged during Li-ion insertion/extraction. To analyze the spectra in detail, we also performed CTM calculations[12–16]. The calculated spectrum is also shown in Fig. 2. Using the parameters for Mn^{2+} high-spin (HS) state with $3d^5$ and $3d^6\underline{L}$ (where, $\underline{L}$ denotes ligand hole) configurations in O_h symmetry[15–19], we could reproduce the experimental XAS. Figure 2 shows a calculated Mn^{2+} HS spectrum with the crystal-field splitting $10Dq$ of 0.8 eV, while the charge-transfer (CT) energy Δ, the on-site $3d$-$3d$ Coulomb energy U_{dd}, and the core-hole potential U_{pd} were respectively fixed to 6.5, 5.2, and 6.2 eV in the calculations. The $10Dq$ of 0.8 eV is smaller than that for $Mn^{II}N_6$ octahedron in MnNCN (∼1 eV)[20]. This is consistent with the weak crystal-field splitting of the $Mn(NC)_{6-\delta}(OH_2)_\delta$ octahedron in MnFe-PBA.

Here, we note the evaporation effect of coordinating water for the Mn $3d$ electronic structure. It is well known that the coordinated water molecules in $Mn(NC)_{6-\delta}(OH_2)_\delta$ can evaporate in vacuum to form $Mn(NC)_{6-\delta}$[21]. Therefore, the estimated $10Dq$ based on the spectra could be slightly different from that for the actual state. Nevertheless, the value on the Mn site was small (0.8 eV) compared to $Mn^{II}N_6$ octahedron (∼ 1 eV)[20]. Therefore, in the present study, the evaporation effect may not be significant.

Figure 3 shows photon-flux-normalized Fe $L_{2,3}$-edge XAS spectra of Li_xMnFe-PBA. The spectrum of MnFe-PBA is similar to that of $K_3[Fe^{III}(CN)_6]$ (Fig. 3(b)), indicating the Fe^{3+} low-spin (LS) states[12,13]. As Li-ion was inserted ($Li_{0.9}$MnFe-PBA), the spectral shape drastically changed and the shape became similar to that of

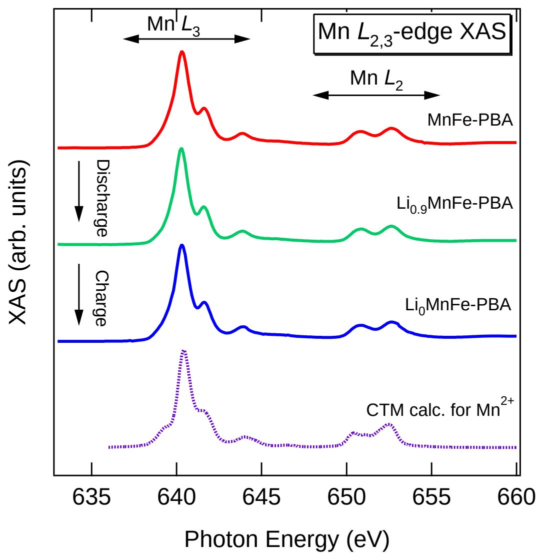

FIG. 2: (Color online) XAS spectra at the Mn $L_{2,3}$-edge of Li_xMnFe-PBA. A CTM-calculated spectrum for Mn^{2+} HS state is also displayed.

$K_4[Fe^{II}(CN)_6]$ (Fig. 3(c))[12,13]. The peak at 706 eV disappeared upon Li-ion insertion can be ascribed to the states consisting mainly of Fe t_{2g} orbital. The other two peaks in the L_3 region (at 709.2 and 710.8 eV) could be attributed to the unoccupied e_g states. Thus, the Fe atoms were reduced as Fe^{3+} LS $\rightarrow$ Fe^{2+} LS by Li-ion insertion. Furthermore, the Fe L-edge spectrum completely returned to the initial shape after Li-ion extraction (Fig. 3(a)). Therefore, the reversible redox reaction occurs mainly on the Fe t_{2g} orbital during Li-ion insertion/extraction.

According to the previous study by Hocking *et al.*[13], the Fe L-edge spectra of $[Fe^{III}(CN)_6]^{3-}$ and $[Fe^{II}(CN)_6]^{4-}$ could be explained only when the metal-to-ligand charge transfer (MLCT) (i.e., π back-donation, Fig. 4(a)) was taken into account in addition to the ligand-to-metal charge transfer (LMCT) (i.e., π/σ back-donation, Fig. 4(a)) in the CTM calculations. Figures 3(b) and 3(c) respectively show the calculated results for Fe^{3+} and Fe^{2+} states with/without MLCT. The Fe L-edge spectra of $[Fe^{III}(CN)_6]^{3-}$ and $[Fe^{II}(CN)_6]^{4-}$ quoted from Ref.[13] are also shown. In the LMCT-only calculation, the parameters of $10Dq = 4.0$ eV, $\Delta = 1.0$ eV, $U_{dd} = 2.0$ eV, and $U_{pd} = 1.0$ eV were used for both Fe^{3+} and Fe^{2+} states. In regard to the LMCT-MLCT combined CTM calculation, the CT energy, i.e., the energy difference between d^n, $d^{n+1}\underline{L}$, and $d^{n-1}L^-$ configurations is given by ground-state energies of EG2 ($d^{n-1}L^-$ and d^n (MLCT)) and EG3 ($d^{n-1}L^-$ and $d^{n+1}\underline{L}$, (relating to LMCT)) and final-state energies EF2 and EF3. The hopping (i.e. mixing) energies for the t_{2g} and e_g symmetries ($V_{t_{2g}}$, V_{e_g}) were also taken into account in the LMCT-MLCT combined CTM calculation[13].

As shown in Fig. 3, the experimental spectra could not be reproduced by the LMCT-only calculations for both Fe^{3+} and Fe^{2+} states, even if the electronic parameters are varied largely. In contrast, the LMCT-MLCT combined calculations well reproduced the spectra. The electronic structure parameters for the best reproduced results are summarized in Table I. This indicated that MnFe-PBA has strong MLCT similar to $K_3[Fe^{III}(CN)_6]$ and $K_4[Fe^{II}(CN)_6]$. However, it should be emphasized that there are slight differences between the Fe L-edge XAS spectra for the isolated complexes ($K_3[Fe^{III}(CN)_6]$ and $K_4[Fe^{II}(CN)_6]$) and coordination polymers (Li_xMnFe-PBA). For example, two peak intensities in the Fe L_3-edge for $Li_{0.9}$MnFe-PBA are almost same. On the other hand, the peak intensity at 710.8 eV is larger than that at 709.2 eV for $K_4[Fe^{II}(CN)_6]$ (Fig. 3(c)). This can be explained by using the LMCT-MLCT combined CTM calculations. By tuning the LMCT and MLCT parameters, e.g. increasing V_{e_g} for LMCT (case 2 in Fig. 3(c)), the peak at 710.8 eV became weaker to reproduce the spectra for $Li_{0.9}$MnFe-PBA. This implied that the σ donating character of CN ligand in $Li_{0.9}$MnFe-PBA is enhanced by the orbital hybridization with Mn.

As for the Fe^{3+} state, the peak intensity at 706 eV for MnFe-PBA is relatively weaker than that for $K_3[Fe^{III}(CN)_6]$ (Fig. 3(b)). As mentioned above, the peak at 706 eV can be attributed to the density of unoccupied states mainly consisting of Fe t_{2g} orbital. Since the Fe t_{2g} orbital well hybridizes with the CN π orbital (Fig. 4(b)), the weaker peak intensity at 706 eV indicates that the π donation to the Fe t_{2g} orbital is larger than that in $K_3[Fe^{III}(CN)_6]$. In other words, $3d^6\underline{L}$ character is enhanced in MnFe-PBA while the σ donating character is enhanced in $Li_{0.9}$MnFe-PBA.

Now, the Fe L-edge XAS for Li_xMnFe-PBA clarified the hybridization between the Fe and CN orbitals, and suggested the enhanced σ/π donation compared to the isolated complexes. Since the strong orbital hybridization should result in the electron delocalization, the changes in the C or N K-edge XAS during the charge/discharge process are also expected. However, changes in the C K-edge XAS among Li_xMnFe-PBA could hardly be observed during Li-ion insertion/extraction because the C K-edge XAS spectra also included a large amount of background signals from acetyleneblack and PTFE (Fig. 5(a)). On the other hand, the N K-edge XAS showed a slight change with Li-ion insertion (Figs. 5(b)). Although it was hard to elucidate quantitatively, the small peak at 397.3 eV, which could be the π orbital hybridized with the Fe t_{2g} orbital, almost disappeared and the main peak of π^* orbital at 400.8 eV decreased with Li-ion insertion. Thus, by Li-ion insertion, the π/π^* orbitals should be reduced in accompany with the Fe t_{2g} orbital, suggesting the electron delocalization on the hybridized Fe t_{2g} and CN π/π^* orbitals. As for the O K-edge XAS studies of TM-oxide such as $Li_{1-x}CoO_2$ and $Li_{1-x}FePO_4$, their spectral changes were much larger than those in the present C and N K-edge XAS[22–24]. This may be due to the difference in the or-

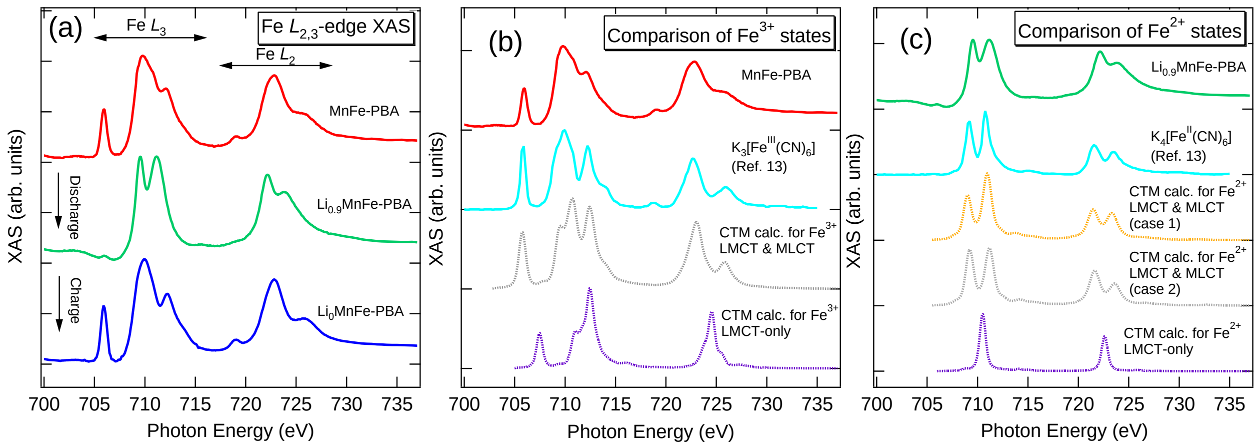

FIG. 3: (Color online) (a) XAS spectra at the Fe $L_{2,3}$-edge of Li_xMnFe-PBA. For comparison, CTM-calculated spectra and the experimental spectra of $K_3[Fe^{III}(CN)_6]$ and $K_4[Fe^{II}(CN)_6]$ quoted from Ref.[13] are also displayed in (b) (for Fe^{3+}) and (c) (for Fe^{2+}). In (c), two LMCT-MLCT combined CTM-calculated spectra with different V_{e_g} in LMCT (1.40 eV for case 1 and 1.85 eV for case 2) are plotted.

bital hybridization mechanism. Since the O $2p$ ($2p_{x,y,z}$) orbitals which form wide band around the Fermi level (E_F) well hybridize any TM $3d$ orbital through the large transfer integrals of $(pd\sigma)$ and $(pd\pi)$ (i.e. σ/π donation), the O K-edge XAS spectra of TM oxides generally include much contribution from the TM's unoccupied $3d$ states in addition to the O $2p$ state[15,25]. For example, the valence band of $LiCoO_2$ (Co^{3+} LS state (t_{2g}^6)), which directly corresponds to the redox behavior ($LiCoO_2 \leftrightarrow Li_{1-x}CoO_2$), was reported to consist of ~37% Co t_{2g} and ~60% O $2p$[23]. Thus, the O K-edge XAS of $Li_{1-x}CoO_2$ has a character of the hole created in the valence band with the strong hybridization, resulting in the large spectral change depending on the Li concentration[22,23]. In contrast, the molecular orbital of CN consists of separated and narrow π/σ bands. The frontier orbital (lowest unoccupied molecular orbital, LUMO) of $[Fe^{3+}(CN)_6]^{3-}$ was reported to consist of 77% Fe t_{2g} and 23% CN π orbitals as a result of LMCT and MLCT[13]. Thus, the small changes in the C and N K-edge XAS should originate from the weak partial density of states of CN on the narrow LUMO. Therefore, the orbital hybridization mechanism in MnFe-PBA (LMCT and MLCT on the narrow CN π band) is different from that in the TM oxides (strong LMCT (σ/π donation) on the wide O $2p$ band). Nevertheless, it is apparent that the hybridization between the Fe and CN orbitals plays an important role in the electronic structure of MnFe-PBA.

Finally, we adress the robustness of MnFe-PBA against the Li-ion insertion/extraction cycles. As Férey *et al.* suggested[6], the charge delocalization during the Li-ion insertion/extraction might be indispensible for the robust and flexible framework for Li-ion storage, since electron localization would induce a large lattice strain that deteriorates the electrode. As for MnFe-PBA, *ex situ* x-ray diffraction measurement revealed that the en-

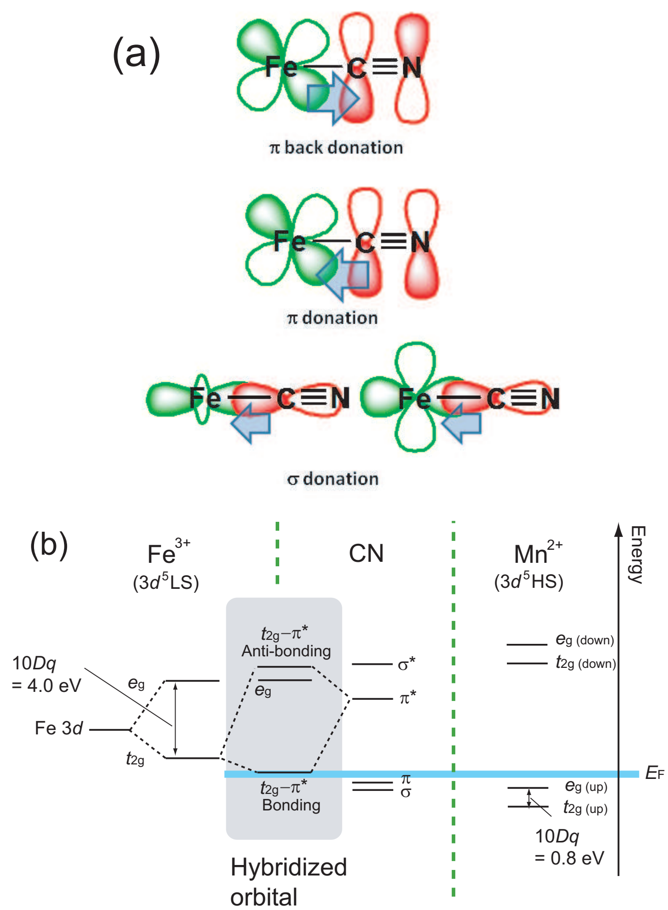

FIG. 4: (Color online) (a) Schematic drawings of the possible CTs between Fe and CN. (b) Energy diagram among the Fe^{3+}, CN, Mn^{2+} states. For simplicity, only the hybridization between the Fe t_{2g} and CN π^* orbitals is depicted.

TABLE I: Electronic structure parameters used in the LMCT-MLCT combined CTM calculations. The relationship between the final- and ground-state energies are given by EF = EG + U_{dd} (3d-3d Coulomb energy) $-U_{pd}$ (core-hole) potential[13].

	$10Dq$	MLCT				LMCT			
		EG2	EF2	$V_{t_{2g}}$	V_{e_g}	EG3	EF3	$V_{t_{2g}}$	V_{e_g}
$Fe^{3+}(3d^5)$ (eV)	4.0	1.0	0.5	0.9	2.0	1.0	1.5	2.1	0.6
$Fe^{2+}(3d^6)$ (eV)	3.7	2.1	1.6	1.4	1.65	-2.0	0.0	1.40 (case 1)	0.6
								1.85 (case 2)	

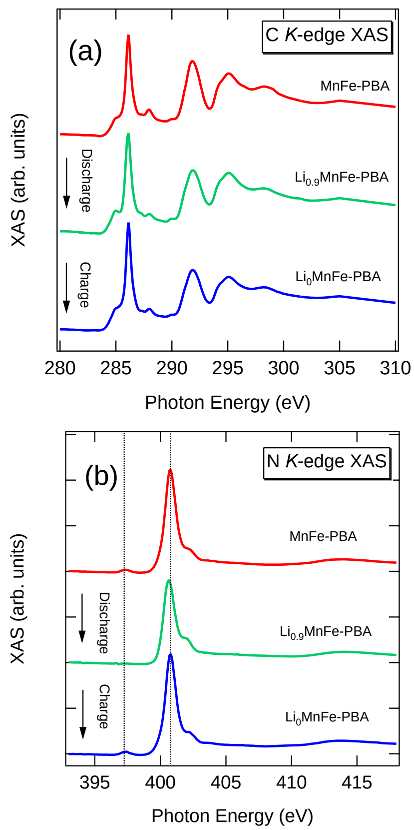

FIG. 5: (Color online) Flux-normalized C (a) and N (b) K-edge XAS.

tire Li-ion insertion/extraction process occurs via a solid solution state, in which the unit cell volume gradually shrinks from 1175.6 to 1136.1 Å(for Li-ion insertion)[7]. The drastic shrinkage/expansion of the lattice (3.4%) apparently indicates the flexibility of the MnFe-PBA framework. As clarified above, the LMCT and MLCT in MnFe-PBA should make the charge delocalize over the Fe and CN orbitals to a certain extent[13,26]. These results proved that the charge delocalization is the origin for the flexibility of MnFe-PBA, and resulting high robustness against Li-ion insertion/extraction (over 100 cycles, Fig. 1(b)), justifying the suggestion by Férey *et al.*[6].

IV. CONCLUSION

XAS was applied to the study on the electronic structure change of MnFe-PBA during various stages of Li-ion insertion/extraction process. The Mn ions were determined to be Mn^{2+} HS state regardless of the Li-ion concentration. CTM calculations revealed that the Mn ions were under the weak crystal field. On the other hand, the Fe L-edge XAS spectra revealed that Li-ion insertion caused redox reaction of Fe^{3+} LS $\leftrightarrow$ Fe^{2+} LS states. The spectral shapes of the Fe^{3+} LS and Fe^{2+} LS states are respectively analogous to those of $K_3[Fe^{III}(CN)_6]$ and $K_4[Fe^{II}(CN)_6]$ of which could be reproduced with MLCT as well as LMCT. However, the degree of LMCT was slightly enhanced by the polymerization. Although the orbital hybridization mechanism was different from that for the TM oxides, the bidirectional CTs between the Fe and CN suggest strong charge delocalization there, leading to the stable Li-ion-storage properties of MnFe-PBA.

This work was financially supported by the Industrial Technology Research Grant Programs in 2009 and 2010 from the New Energy and Industrial Development Organization (NEDO), Japan. This work was done under the approval of the Photon Factory Program Advisory Committee (Proposal No. 2010G038). This work was also conducted based on the MOU between AIST, Japan and LBNL, DOE, USA. The Advanced Light Source is supported by the Director, Office of Science, Office of Basic Energy Sciences of the U.S. Department of Energy under Contract No. DE-AC02-05CH11231.

[1] H. Furukawa *et al.*, Science **329**, 424 (2010).
[2] G. J. Halder *et al.*, Science **298**, 1762 (2002).
[3] S. Kitagawa, R. Kitaura, and S.-i. Noro, Angew. Chem. Int. Ed. **43**, 2334 (2004).
[4] N. Imanishi *et al.*, J. Power Sources **79**, 215 (1999).
[5] N. Imanishi *et al.*, J. Power Sources **81**, 530 (1999).
[6] G. Férey *et al.*, Angew. Chem. Int. Ed. **46**, 3259 (2007).
[7] M. Okubo *et al.*, J. Phys. Chem. Lett. **1**, 2063 (2010).
[8] T. Yokoyama *et al.*, Phys. Rev. B **66**, 184111 (2002).
[9] H. Tokoro *et al.*, Phys. Rev. B **73**, 172415 (2006).
[10] H. Tokoro, S.-i. Ohkoshi, and K. Hashimoto, Appl. Phys. Lett. **82**, 1245 (2003).
[11] C. Tian *et al.*, Inorg. Chem. **49**, 3086 (2010).
[12] C. Cartier dit Moulin *et al.*, J. Am. Chem. Soc. **122**, 6653 (2000).
[13] R. K. Hocking *et al.*, J. Am. Chem. Soc. **128**, 10442 (2006).
[14] E. Coronado *et al.*, J. Am. Chem. Soc. **130**, 15519 (2008).
[15] F. M. F. de Groot and A. Kotani, *Core Level Spectroscopy of Solids*, Advances in Condensed Matter Science (CRC Press, Boca Raton, FL, 2008).
[16] F. M. F. de Groot, J. Electron Spectrosc. Relat. Phenom. **62**, 111 (1993).
[17] F. M. F. de Groot *et al.*, Phys. Rev. B **42**, 5459 (1990).
[18] G. van der Laan and I. W. Kirkman, J. Phys.: Condens. Matter **4**, 4189 (1992).
[19] F. M. F. de Groot, J. Electron Spectrosc. Relat. Phenom. **67**, 529 (1994).
[20] X. Liu *et al.*, Z. Anorg. Allg. Chem. **636**, 343 (2010).
[21] R. Martinez-Gracia, M. Knobel, and E. Reguera, J. Phys.: Condens. Matter **18**, 11243 (2006).
[22] W.-S. Yoon *et al.*, J. Phys. Chem. B **106**, 2526 (2002).
[23] M. T. Czyżyk, R. Potze, and G. A. Sawatzky, Phys. Rev. B **46**, 3729 (1992).
[24] A. Augustsson *et al.*, J. Chem. Phys. **123**, 184717 (2005).
[25] M. Imada, A. Fujimori, and Y. Tokura, Rev. Mod. Phys. **70**, 1039 (1998).
[26] R. K. Hocking *et al.*, J. Am. Soc. **129**, 113 (2007).